Computers and Mathematics with Applications 68 (2014) 174–184

Contents lists available at ScienceDirect

Computers and Mathematics with Applications

journal homepage: www.elsevier.com/locate/camwa

A semi-analytical Fourier spectral method for the Allen–Cahn equation

Hyun Geun Lee [a], June-Yub Lee [b,*]

[a] Institute of Mathematical Sciences, Ewha Womans University, Seoul 120-750, Republic of Korea
[b] Department of Mathematics, Ewha Womans University, Seoul 120-750, Republic of Korea

ARTICLE INFO

Article history:
Received 30 December 2013
Received in revised form 4 May 2014
Accepted 15 May 2014
Available online 6 June 2014

Keywords:
Phase-field method
Stabilized semi-implicit Fourier spectral method
Unconditional stability
First and second order convergence

ABSTRACT

In recent years, Fourier spectral methods have been widely used as a powerful tool for solving phase-field equations. To improve its effectiveness, many researchers have employed stabilized semi-implicit Fourier spectral (SIFS) methods which allow a much larger time step than a usual explicit scheme. Our mathematical analysis and numerical experiments, however, suggest that an effective time step is smaller than a time step specified in the SIFS schemes. In consequence, the SIFS scheme is inaccurate for a considerably large time step and may lead to incorrect morphologies in phase separation processes. In order to remove the time step constraint and guarantee the accuracy in time for a sufficiently large time step, we present a first and a second order semi-analytical Fourier spectral (SAFS) methods for solving the Allen–Cahn equation. The core idea of the methods is to decompose the original equation into linear and nonlinear subequations, which have closed-form solutions in the Fourier and physical spaces, respectively. Both the first and the second order methods are unconditionally stable and numerical experiments demonstrate that our proposed methods are more accurate than the stabilized semi-implicit Fourier spectral method.

1. Introduction

The phase-field method has recently emerged as a powerful computational approach for modeling and predicting mesoscale morphological and microstructure evolution in materials. This method replaces sharp interfaces by thin but nonzero thickness transition regions where the interfacial forces are smoothly distributed [1]. The basic idea is to introduce conserved or non-conserved order parameters ϕ that vary continuously over thin interfacial layers and are mostly uniform in the bulk phases. The temporal and spatial evolution of the order parameters is governed by the Cahn–Hilliard equation [2–10] or the Allen–Cahn (AC) equation [11–15]. The most significant computational advantage of the phase-field method is that an explicit tracking of the interface is unnecessary.

Numerous numerical algorithms have been developed to improve the accuracy and numerical stability of the phase-field method. There are two types of approaches to achieve high spatial accuracy. One is the adaptive mesh refinement method [16–18] in which additional grid points are placed in regions where the order parameters have large gradients, and the other is the Fourier spectral method [19–30] which uses a spectral representation of a continuous spatial profile of the order parameter. The Fourier spectral method is good for evaluating spatial derivatives since the differential operators are

* Corresponding author.
E-mail address: jyllee@ewha.ac.kr (J.-Y. Lee).

http://dx.doi.org/10.1016/j.camwa.2014.05.015
0898-1221/

represented in the transform space by diagonal matrices that are trivially inverted. Here, we focus on the Fourier spectral method.

To improve the effectiveness of the Fourier spectral method, many researchers have employed stabilized semi-implicit schemes [21,23,24,26,28–30] for the time variable, in which the principal elliptic operator is treated implicitly to reduce the associated stability constraint, while the nonlinear term is still treated explicitly to avoid the expensive process of solving nonlinear equations at each time step [19]. And an extra stabilizing term is added to improve the stability while preserving the simplicity. Stabilized semi-implicit schemes alleviate the time step restriction of explicit schemes, i.e., enable us to use a considerably large time step. But, we observed, through both mathematical analysis and numerical examples, that if we use a large time step, then an effective time step becomes smaller than a time step specified in the stabilized semi-implicit scheme. (Cheng and Rutenberg [31] also pointed out this problem.) In consequence, the stabilized semi-implicit scheme is inaccurate, leading to incorrect morphologies in phase separation processes.

To allow the use of a sufficiently large time step with neither loss of accuracy nor technical difficulty, we present a first and a second order (in time) semi-analytical Fourier spectral methods for solving the AC equation. A core idea of this method is to decompose the original equation into linear and nonlinear subequations, which have closed-form solutions in the Fourier and physical spaces, respectively. In particular, our method requires no additional computational cost and is unconditionally stable in the sense that the solution remains to be bounded for all time regardless of the time step size. It can be used to solve various modified forms of the AC equation such as crystal growth [32,33], grain growth [34–36], and image analysis [37–44].

This paper is organized as follows. In Section 2, we present a first order semi-analytical Fourier spectral method for the AC equation and prove the unconditional stability of this method. We present numerical experiments of the first order stabilized semi-implicit and semi-analytical schemes in Section 3. In Section 4, we introduce the second order stabilized semi-implicit and semi-analytical schemes, and present numerical experiments of both schemes. Conclusions are drawn in Section 5.

2. A semi-analytical Fourier spectral method

We consider the AC equation in two-dimensional space:

$$\frac{\partial \phi(\mathbf{x},t)}{\partial t} = \frac{\phi(\mathbf{x},t) - \phi^3(\mathbf{x},t)}{\epsilon^2} + \Delta\phi(\mathbf{x},t), \quad \mathbf{x} \in \Omega,\ 0 < t \le T, \tag{1}$$

where $\mathbf{x} = (x_1, x_2)$ is a point inside a rectangular domain $\Omega = (0, L_1) \times (0, L_2)$. The boundary condition is the zero Neumann boundary condition:

$$\nabla\phi \cdot \mathbf{n} = 0 \quad \text{on } \partial\Omega, \tag{2}$$

where $\mathbf{n}$ is the unit normal vector to $\partial\Omega$. Instead of using a finite difference approximation, we propose using a Fourier spectral approximation to the AC equation. To solve the AC equation with the boundary condition (2), we employ the discrete cosine transform [45]: for $k_1 = 0, \ldots, N_1 - 1$ and $k_2 = 0, \ldots, N_2 - 1$,

$$\widehat{\phi}_{k_1k_2} = \alpha_{k_1}\beta_{k_2} \sum_{l_1=0}^{N_1-1} \sum_{l_2=0}^{N_2-1} \phi_{l_1l_2} \cos\left[\frac{\pi}{N_1} k_1 \left(l_1 + \frac{1}{2}\right)\right] \cos\left[\frac{\pi}{N_2} k_2 \left(l_2 + \frac{1}{2}\right)\right],$$

where $\alpha_0 = \sqrt{1/N_1}$, $\beta_0 = \sqrt{1/N_2}$, $\alpha_{k_1} = \sqrt{2/N_1}$, $\beta_{k_2} = \sqrt{2/N_2}$ if $k_1, k_2 \ge 1$, and $\phi_{l_1l_2} = \phi\left(\frac{L_1}{N_1}\left(l_1 + \frac{1}{2}\right), \frac{L_2}{N_2}\left(l_2 + \frac{1}{2}\right)\right)$. Then, Eq. (1) can be transformed into a set of ordinary differential equations in the cosine space:

$$\frac{\partial \widehat{\phi}_{k_1k_2}}{\partial t} = \frac{\widehat{\phi}_{k_1k_2} - \widehat{\phi^3}_{k_1k_2}}{\epsilon^2} + A_{k_1k_2}\widehat{\phi}_{k_1k_2}, \tag{3}$$

where $A_{k_1k_2} = -\pi^2\left[\left(\frac{k_1}{L_1}\right)^2 + \left(\frac{k_2}{L_2}\right)^2\right]$.

An Explicit Fourier Spectral (ExFS) method is to approximate (3) by

$$\widehat{\phi}^{n+1}_{k_1k_2} = \widehat{\phi}^{n}_{k_1k_2} + \Delta t\left(\frac{\widehat{\phi}^{n}_{k_1k_2} - \widehat{(\phi^n)^3}_{k_1k_2}}{\epsilon^2} + A_{k_1k_2}\widehat{\phi}^{n}_{k_1k_2}\right). \tag{4}$$

This method offers excellent spatial accuracy, but it is only first order accurate in time and suffers from the severe time step restriction for stability. To overcome this problem, many researchers have used the first order stabilized Semi-Implicit Fourier Spectral (SIFS) method [26,28,29]:

$$\left(1 - \Delta t A_{k_1k_2} + \frac{S\Delta t}{\epsilon^2}\right)\widehat{\phi}^{n+1}_{k_1k_2} = \widehat{\phi}^{n}_{k_1k_2} + \Delta t\frac{(S+1)\widehat{\phi}^{n}_{k_1k_2} - \widehat{(\phi^n)^3}_{k_1k_2}}{\epsilon^2}, \tag{5}$$

where $S(>0)$ is the stabilization parameter. In (5), an extra dissipative term $\frac{S\Delta t}{\epsilon^2}\left(\widehat{\phi}^{n+1}_{k_1k_2}-\widehat{\phi}^{n}_{k_1k_2}\right)$ is introduced to improve the stability while preserving the simplicity. The stabilized semi-implicit treatment allows us to use a sufficiently large time step. Eq. (5) implicitly defines the updated phase-field $\widehat{\phi}^{n+1}_{k_1k_2}$ and can be directly solved in Fourier space to give a Euler-like update

$$\widehat{\phi}^{n+1}_{k_1k_2}=\widehat{\phi}^{n}_{k_1k_2}+\frac{\Delta t}{1-\Delta tA_{k_1k_2}+\frac{S\Delta t}{\epsilon^2}}\left(\frac{\widehat{\phi}^{n}_{k_1k_2}-\widehat{(\phi^n)^3}_{k_1k_2}}{\epsilon^2}+A_{k_1k_2}\widehat{\phi}^{n}_{k_1k_2}\right). \tag{6}$$

Eq. (6) can be viewed as an explicit method in the form of (4) with a k_1k_2-dependent effective time step Δt_{eff},

$$\Delta t_{\text{eff}}:=\frac{\Delta t}{1-\Delta tA_{k_1k_2}+\frac{S\Delta t}{\epsilon^2}}\le\Delta t_{\text{critical}}:=\frac{\Delta t}{1+\frac{S\Delta t}{\epsilon^2}}. \tag{7}$$

This implies that $\Delta t_{\text{eff}}\to\Delta t$ as $\Delta t\to 0$ which provides the consistency and $\Delta t_{\text{eff}}\le\Delta t_{\text{critical}}<\frac{\epsilon^2}{S}$ which guarantees the stability of the method. However, the accuracy is significantly lost for a large time step size since $\Delta t_{\text{eff}}\ll\Delta t$ for $\Delta t\gg\frac{\epsilon^2}{S}$. We will discuss this in more detail in Section 3.

To remove the time step constraint and guarantee the accuracy in time for a sufficiently large time step, we propose a Semi-Analytical Fourier Spectral (SAFS) method. In this scheme, we decompose (1) into linear and nonlinear subequations on each time step:

$$\frac{\phi^*_{l_1l_2}-\phi^n_{l_1l_2}}{\Delta t}=\Delta\phi^*_{l_1l_2}, \tag{8}$$

$$\frac{\phi^{n+1}_{l_1l_2}-\phi^*_{l_1l_2}}{\Delta t}=\frac{\phi^{n+1}_{l_1l_2}-(\phi^{n+1}_{l_1l_2})^3}{\epsilon^2}, \tag{9}$$

where $\phi^*_{l_1l_2}$ is an intermediate solution obtained by solving the linear subequation (8). Eq. (8) can be considered as the first order implicit discretization of the equation $\phi_t=\Delta\phi$ with an initial condition ϕ^n, which has the following analytic form of the solution in Fourier space:

$$\widehat{\phi}^*_{k_1k_2}=e^{A_{k_1k_2}\Delta t}\widehat{\phi}^n_{k_1k_2}. \tag{10}$$

Next, Eq. (9) can also be considered as the first order implicit discretization of the equation $\phi_t=\frac{\phi-\phi^3}{\epsilon^2}$ with an initial condition ϕ^*, which can be integrated analytically in the physical space and the exact solution at $t^{n+1}=t^n+\Delta t$ is given [15,28] as follows:

$$\phi^{n+1}(\mathbf{x})=\frac{\phi^*(\mathbf{x})}{\sqrt{e^{\frac{-2\Delta t}{\epsilon^2}}+(\phi^*(\mathbf{x}))^2\left(1-e^{\frac{-2\Delta t}{\epsilon^2}}\right)}}. \tag{11}$$

In the SAFS method, the solution ϕ^{n+1} of the AC equation at $(n+1)$-th time step can be obtained using ϕ^n by the following two sub-steps:

STEP1. Applying the discrete cosine transform to $\phi^n_{l_1l_2}$, we have $\widehat{\phi}^*_{k_1k_2}$ by (10). Finally, we return to the physical space by applying the inverse discrete cosine transform,

$$\phi^*_{l_1l_2}=\mathcal{C}^{-1}\left[e^{A_{k_1k_2}\Delta t}\mathcal{C}\left[\phi^n_{l_1l_2}\right]\right],$$

where $\mathcal{C}$ denotes the discrete cosine transform and $\mathcal{C}^{-1}$ its inverse.

STEP2. We get the solution $\phi^{n+1}_{l_1l_2}$ by the nonlinear time integration (11),

$$\phi^{n+1}_{l_1l_2}=\frac{\phi^*_{l_1l_2}}{\sqrt{e^{\frac{-2\Delta t}{\epsilon^2}}+(\phi^*_{l_1l_2})^2\left(1-e^{\frac{-2\Delta t}{\epsilon^2}}\right)}}$$

with the intermediate solution $\phi^*_{l_1l_2}$ obtained in the first step.

It is obvious that the proposed method is unconditionally stable in the sense that the solution remains to be bounded by 1 for all time. In the first step, a function defined as a cosine series

$$\psi^{\Delta t}(x_1,x_2):=\sum_{k_1=0}^{N_1-1}\sum_{k_2=0}^{N_2-1}e^{A_{k_1k_2}\Delta t}\widehat{\psi^0}_{k_1k_2}\cos\left(\frac{\pi}{N_1}k_1x_1\right)\cos\left(\frac{\pi}{N_2}k_2x_2\right)$$

is a solution of the heat equation with an initial condition $\psi^0(x_1, x_2)$ thus satisfies the maximum principle, $\max_{x_1,x_2} |\psi^{\Delta t}(x_1, x_2)| \le \max_{x_1,x_2} |\psi^0(x_1, x_2)|$. Therefore,

$$\max_{l_1,l_2} |\phi^*_{l_1l_2}| = \max_{x_1,x_2} |\phi^*(x_1, x_2)| \le \max_{x_1,x_2} |\phi^n(x_1, x_2)| = \max_{l_1,l_2} |\phi^n_{l_1l_2}|.$$

In the second step, if we assume that $|\phi^*_{l_1l_2}| \le 1$ for each l_1, l_2 then

$$|\phi^{n+1}_{l_1l_2}| = \frac{|\phi^*_{l_1l_2}|}{\sqrt{(\phi^*_{l_1l_2})^2 + \left(1 - (\phi^*_{l_1l_2})^2\right) e^{\frac{-2\Delta t}{\epsilon^2}}}} \le 1.$$

Therefore, the proposed method is unconditionally stable regardless of the time step size since $\max_{l_1,l_2} |\phi^{n+1}_{l_1l_2}| \le 1$ for given $\max_{l_1,l_2} |\phi^n_{l_1l_2}| \le 1$.

3. Numerical experiments

In this section, we present two examples (traveling wave solution in 1D and spinodal decomposition in 2D) in order to numerically demonstrate the stability and convergence of the proposed semi-analytical Fourier spectral (SAFS) method compared to the well-known stabilized semi-implicit Fourier spectral (SIFS) method with $S = 2$.

3.1. Traveling wave solutions

One of the well-known traveling wave solutions of the Allen–Cahn equation is

$$\phi(x, t) = \frac{1}{2}\left(1 - \tanh\frac{x - 0.5 - st}{2\sqrt{2}\epsilon}\right), \tag{12}$$

where $s = 3/(\sqrt{2}\epsilon)$ is the speed of the traveling wave. Using this traveling wave solution, we compare the proposed semi-analytical Fourier spectral method with explicit Fourier spectral (ExFS) and stabilized semi-implicit Fourier spectral methods. We set $\epsilon = 0.03\sqrt{2}$ and compute $\phi(x, t)$ for $0 < t \le T_f = 1/s$ with an initial condition $\phi(x, 0)$ on the domain $\Omega = [0, 4]$. The numerical solutions are obtained by the ExFS, SIFS, and SAFS methods with various time step sizes Δt but the spatial grid size is fixed to $h = 2^{-5}$ which provides enough spatial accuracy.

Fig. 1 shows a table for the relative discrete l_2 errors of the numerical solutions $\phi(x, T_f)$ for different time step sizes and two plots for the computed results with $\Delta t/T_f = 2^{-7}$ and 2^{-3}. All three methods show the first order convergence when Δt is small enough, say $\Delta t/T_f < 2^{-7}$. The ExFS method, however, has severe stability constraint and $\Delta t/T_f = 2^{-7}$ is close to the maximum time step to maintain numerical stability for $\epsilon = 0.03\sqrt{2}$ while $\Delta t/T_f = 2^{-3}$ is still a stable choice for both the SIFS and the SAFS methods. When Δt is getting bigger, say $\Delta t/T_f = 2^{-7}$ or 2^{-3}, the simulations indicate that the results obtained from the SIFS method travel with a wrong speed unlike the SAFS method, which phenomenon needs to be further investigated.

To clarify the effect of slow moving speed of the SIFS solution, we check an interfacial x position which corresponds to the 0.5-level of numerical solution for different time steps. Let $x^I(T_f)$ be an interfacial point where $\phi(x^I, T_f) = 0.5$ and the final time $T_f = 1/s$ was chosen to make the x position of the exact solution to be 1.5. Fig. 2(a) shows the absolute values of the differences between the exact x^I position (=1.5) and the numerical x^I position with the SIFS and SAFS methods for different time steps. Both methods provide the first order convergence as expected when Δt is small; however, the SIFS method has significant error when $\Delta t/T_f > 2^{-5}$ or roughly $\Delta t > 10^{-3}$. As the time step increases, the difference between the x position of the SIFS method and the exact position 1.5 becomes bigger and bigger.

Fig. 2(b) shows the numbers of time steps for a numerical solution to reach the interfacial position $x^I = 1.5$ as a function of time step size. The number of time steps for the SAFS method is $T_f/\Delta t$ as expected; however, the number of time steps for the SIFS method is not approaching to 1 as $\Delta t \to T_f$. This means that the effective time step size of the SIFS method for a large time step size is much smaller than the time step size used. The numerical simulation confirms that the number of required time steps can be well estimated by $\Delta t_{\text{critical}}$ defined in (7),

$$N_{\text{steps}} \approx \frac{T_f}{\Delta t_{\text{eff}}} \ge \frac{T_f}{\Delta t_{\text{critical}}} = \frac{T_f}{\Delta t} + T_f\frac{S}{\epsilon^2},$$

where $T_f\frac{S}{\epsilon^2}$ in this simulation is $\frac{\sqrt{2}\epsilon}{3}\frac{2}{\epsilon^2} = \frac{200}{9}$.

Fig. 3 shows the number of time steps to make the numerical solutions reach the correct interfacial position. In order to see the number of time steps only as a function of interface thickness parameter ϵ, we choose $T_f = 1/s = \sqrt{2}\epsilon/3$, $x^I(T_f) = 1.5$, and $\Delta t = T_f/10$ or $\Delta t = T_f/1$. The numerical simulation clearly shows that N_{steps} of the SIFS method can be well estimated by $\frac{T_f}{\Delta t_{\text{critical}}} = \frac{T_f}{\Delta t} + \frac{\sqrt{2}}{3}\frac{S}{\epsilon}$ while N_{steps} of the SAFS method is simply $\frac{T_f}{\Delta t}$.

$\Delta t/T_f$	2^{-11}	2^{-9}	2^{-7}	2^{-5}	2^{-3}
ExFS method	4.6729e–3	1.8476e–2	7.0354e–2	unstable	unstable
SIFS method	1.7044e–2	6.5457e–2	2.1761e–1	4.7416e–1	6.6772e–1
SAFS method	1.2188e–4	4.8671e–4	1.9334e–3	7.5161e–3	2.6270e–2

(a) Relative l_2 errors of $\phi(x, T_f)$ for various time step sizes.

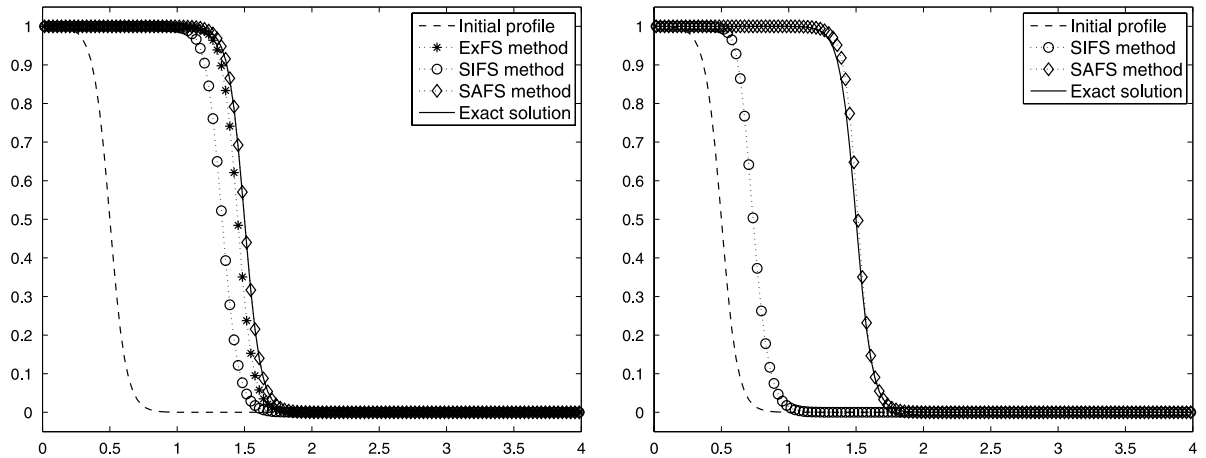

(b) $\Delta t/T_f = 2^{-7}$. (c) $\Delta t/T_f = 2^{-3}$.

Fig. 1. Computational results of the traveling wave solution $\phi(x, T_f)$ at $T_f = 1/s$ with $\epsilon = 0.03\sqrt{2}$ and $h = 2^{-5}$. (a) Relative l_2 errors for the ExFS, the SIFS, and the SAFS methods for various time step sizes. (b) Comparison of the results for $\Delta t/T_f = 2^{-7}$. (c) Comparison of the results for $\Delta t/T_f = 2^{-3}$.

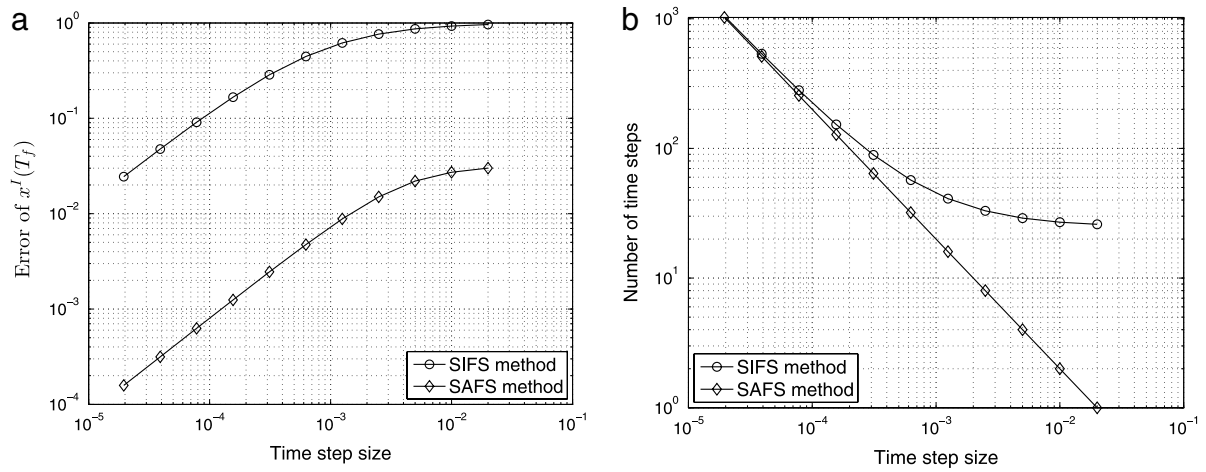

Fig. 2. Interfacial position $x^I(T_f)$ of numerical solutions at $T_f = 1/s$ with $\epsilon = 0.03\sqrt{2}$ for various time step sizes. (a) Errors of the numerical $x^I(T_f)$ position. (b) Numbers of time steps required for a numerical solution to reach $x^I = 1.5$.

3.2. Spinodal decomposition

The Allen–Cahn equation also arises [46] from minimization of the Ginzburg–Landau free energy

$$\mathcal{E}(\phi) := \int_\Omega \left(\frac{F(\phi)}{\epsilon^2} + \frac{|\nabla\phi|^2}{2} \right) d\mathbf{x},$$

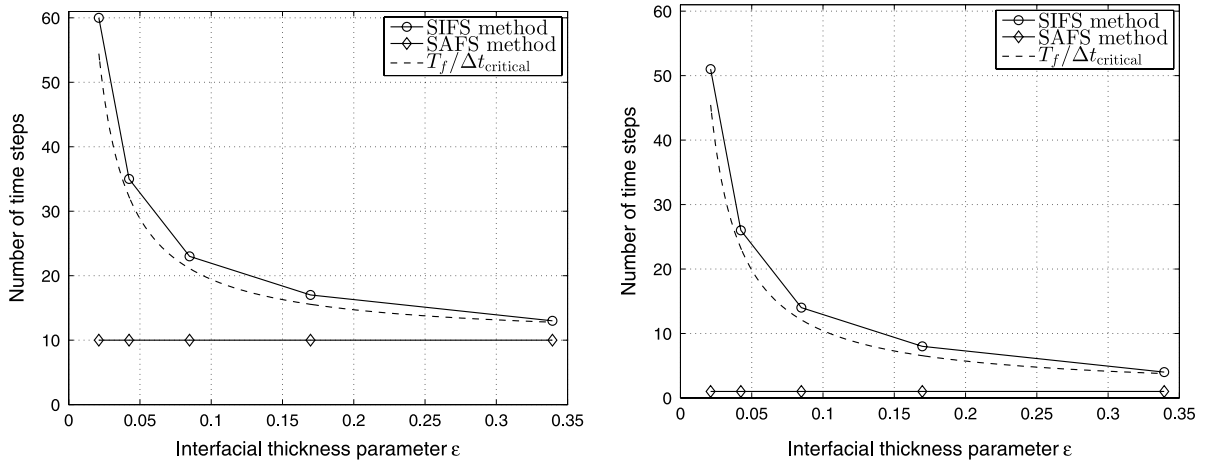

(a) $\Delta t = T_f/10$. (b) $\Delta t = T_f/1$.

Fig. 3. Numbers of required time steps for the first order SIFS solution ($S = 2$) to reach $x^l = 1.5$ with $T_f = 1/s = \sqrt{2}\epsilon/3$ as a function of thickness parameter ϵ.

where $F(\phi) = 0.25(1-\phi^2)^2$ is the bulk free energy having a double well form. The AC equation is the L^2-gradient flow of the total free energy $\mathcal{E}(\phi)$:

$$\frac{\partial \phi}{\partial t} = -\text{grad}\mathcal{E}(\phi), \tag{13}$$

where the symbol "grad" denotes the gradient on the manifold in $L^2(\Omega)$ space. Let the domain of definition for the functional $\mathcal{E}$ be $\mathcal{D} = \{\phi \in H^2(\Omega) \mid \frac{\partial \phi}{\partial \mathbf{n}} = 0 \text{ on } \partial\Omega\}$. Let $\phi, \psi \in \mathcal{D}$. Then, we have

$$\begin{aligned}(\text{grad}\mathcal{E}(\phi), \psi)_{L^2} &= \frac{d}{d\theta}\mathcal{E}(\phi + \theta\psi)\Big|_{\theta=0} = \lim_{\theta\to 0}\frac{1}{\theta}(\mathcal{E}(\phi+\theta\psi) - \mathcal{E}(\phi)) \\ &= \int_\Omega \left(\frac{F'(\phi)}{\epsilon^2} - \Delta\phi\right)\psi d\mathbf{x} = \left(\frac{F'(\phi)}{\epsilon^2} - \Delta\phi, \psi\right)_{L^2},\end{aligned}$$

where we have used integration by parts and the boundary condition (2). We identify $\text{grad}\mathcal{E}(\phi) \equiv F'(\phi)/\epsilon^2 - \Delta\phi$; then (13) becomes the AC equation.

For $\phi_1 = -1/\sqrt{3}$ and $\phi_2 = 1/\sqrt{3}$, $F''(\phi) > 0$ for $-1 < \phi < \phi_1$ or $\phi_2 < \phi < 1$ and $F''(\phi) < 0$ for $\phi_1 < \phi < \phi_2$. The intervals $(-1, \phi_1)$ and $(\phi_2, 1)$ are called metastable intervals and (ϕ_1, ϕ_2) is called the spinodal interval [47]. It is known that ϕ which lies in the spinodal interval is very unstable and that the growth of instabilities results in phase separation, which is called spinodal decomposition. In this subsection, we perform a spinodal decomposition computation to compare the SAFS method with the SIFS method for different time steps. We set $\epsilon = 0.015$, $h = 1/128$ on the domain $\Omega = [0,1]\times[0,1]$ and the initial condition is $\phi(x, y, 0) = 0.005 \cdot \text{rand}(x, y)$ where $\text{rand}(x, y)$ is a random number between -1 and 1.

Fig. 4 shows evolutions of the numerical solution $\phi(x, y, t)$ using the SIFS and SAFS methods for different time steps. Rows 1, 2, and 3 show snapshots of the solution obtained from the SIFS method at different times for $\Delta t = 5\cdot 10^{-4}, 5\cdot 10^{-5}$, and $5\cdot 10^{-6}$, respectively. Row 4 shows snapshots of the solution obtained from the SAFS method at different times for $\Delta t = 5\cdot 10^{-4}$. The results in Fig. 4 show that the SIFS method is robust but significantly inaccurate for a larger time step size, leading to incorrect morphologies in the phase separation process, while there are nearly no significant differences of the SAFS solutions with $\Delta t \le 5\cdot 10^{-4}$ compared to the results plotted with the coarsest time step. It is worthwhile to note that the SIFS method experiences a slow evolution side effect as Δt is getting bigger and the solution computed with $\Delta t = 5\cdot 10^{-4}$ at $t = 6\cdot 10^{-3}$ is quite similar with the converged solution at $t = 10^{-3}$. In fact, the slow-down factor defined as

$$\frac{\Delta t}{\Delta t_{\text{eff}}} \approx \frac{\Delta t}{\Delta t_{\text{critical}}} = 1 + S\frac{\Delta t}{\epsilon^2} \tag{14}$$

is $5\frac{4}{9} \approx 5.444$ for the computation with $\Delta t = 5\cdot 10^{-4}$ and $\epsilon = 0.015$. This simulation numerically demonstrates that the SAFS method has no slow-down side effect and is significantly more accurate than the widely used SIFS method for solving phase-field equations.

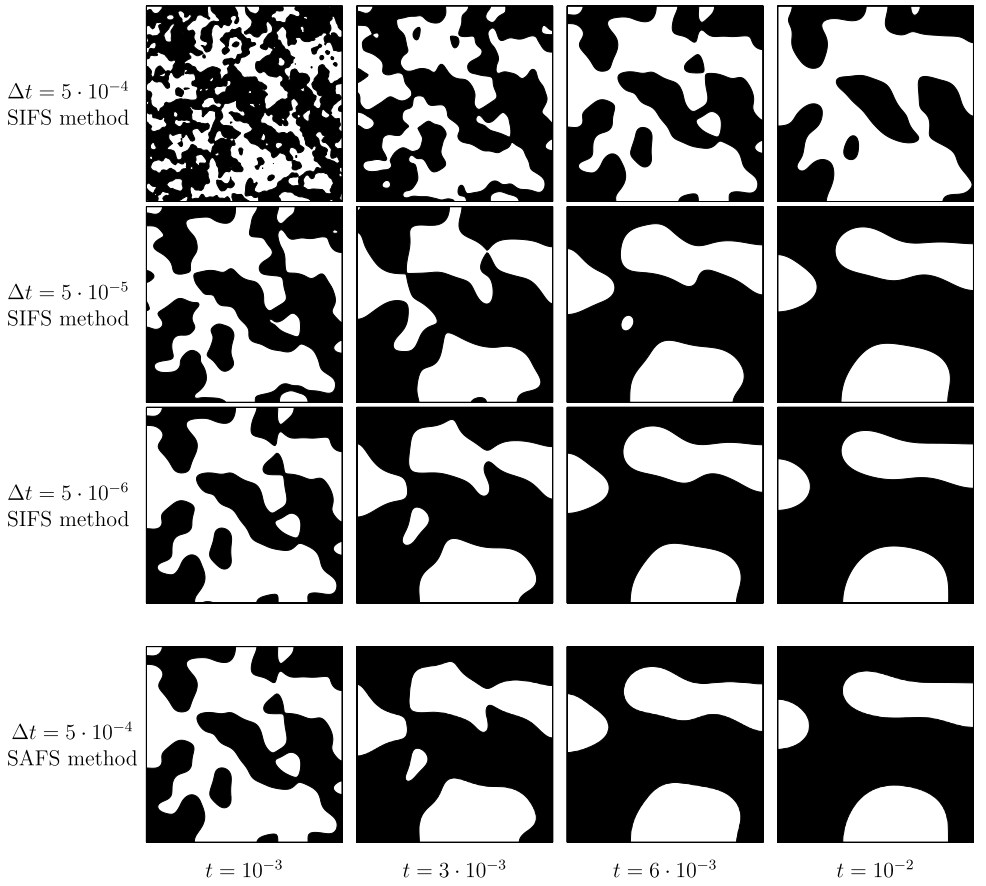

Fig. 4. Spinodal decomposition of the numerical solution $\phi(x, y, t)$ obtained from the SIFS and SAFS methods. Each row of the figure shows snapshots of the solution at the times indicated at the bottom and is calculated using the time step indicated on the left hand side of the figure.

4. Second order Fourier spectral methods

One of the important merits of using the Semi-Analytical Fourier Spectral (SAFS) method is the flexibility to develop temporally high order methods by combining operator splitting steps. We present a second order SAFS method which combines a half-time linear solver and a full-time nonlinear solver followed by a final half-time linear solver:

$$\phi^n = \phi(\mathbf{x}, t^n) \xrightarrow{\phi_t = \Delta\phi} \phi^* := \phi\left(\mathbf{x}, t^n + \frac{\Delta t}{2}\right), \tag{15}$$

$$\phi^* = \phi(\mathbf{x}, t^n) \xrightarrow{\phi_t = (\phi - \phi^3)/\epsilon^2} \phi^{**} := \phi(\mathbf{x}, t^n + \Delta t), \tag{16}$$

$$\phi^{**} = \phi\left(\mathbf{x}, t^n + \frac{\Delta t}{2}\right) \xrightarrow{\phi_t = \Delta\phi} \phi^{n+1} := \phi(\mathbf{x}, t^n + \Delta t), \tag{17}$$

where ϕ^* and ϕ^{**} are the intermediate solutions by solving the subequations on the top of the arrows with the initial conditions on the left of the arrows in (15) and (16), respectively. Eqs. (15) and (17) are similar to (8) and can be solved in a similar way. Also (16) is similar to (9) and can be solved in a similar way. This method is merely an implementation of the operator splitting schemes and provides a second order convergence [28] since each of the sub-steps is computed semi-analytically. The second order method is unconditionally stable and the proof of the stability is trivial if we follow the argument at the end of Section 2.

In this section, we present three numerical examples (again the traveling wave solution in 1D, motion by mean curvature in 2D, and spinodal decomposition 3D) in order to demonstrate the numerical convergence and stability of the method. For the comparison purpose, we also provide numerical solutions by the well-known second-order stabilized semi-implicit Fourier spectral (SIFS) method defined as follows,

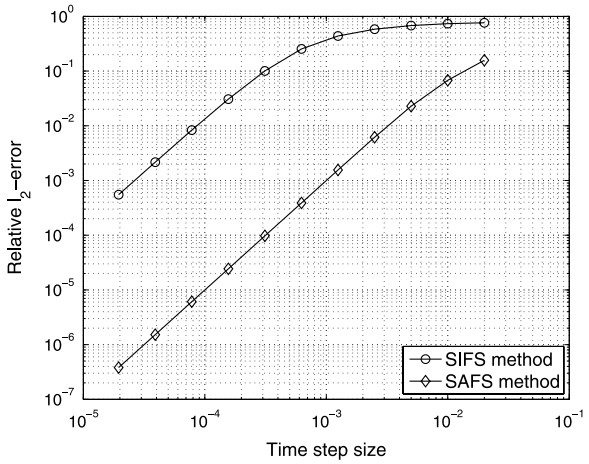

Fig. 5. Relative l_2 errors of the traveling wave solution at $T_f = 1/s$ by the SIFS and the SAFS methods for various time step sizes with $h = 2^{-5}$ and $\epsilon = 0.03\sqrt{2}$.

$$\left(\frac{3}{2} - \Delta t A_{k_1k_2} + \frac{S\Delta t}{\epsilon^2}\right)\widehat{\phi}^{n+1}_{k_1k_2} = 2\widehat{\phi}^{n}_{k_1k_2} + 2\Delta t\frac{(S+1)\widehat{\phi}^{n}_{k_1k_2} - \widehat{(\phi^n)^3}_{k_1k_2}}{\epsilon^2} - \frac{1}{2}\widehat{\phi}^{n-1}_{k_1k_2} - \Delta t\frac{(S+1)\widehat{\phi}^{n-1}_{k_1k_2} - \widehat{(\phi^{n-1})^3}_{k_1k_2}}{\epsilon^2}. \tag{18}$$

4.1. Traveling wave solutions

We solve the AC equation by the second order SAFS method defined in (15)–(17) to obtain the traveling wave solutions $\phi(x,t) = \frac{1}{2}\left(1 - \tanh\frac{x-0.5-st}{2\sqrt{2}\epsilon}\right)$ with the speed of the traveling wave $s = 3/(\sqrt{2}\epsilon)$. For the comparison purpose, we use the second order SIFS method defined in (18) with $S = 2$. Fig. 5 shows the computational error of the numerical solutions at $T_f = 1/s$ by the SIFS and SAFS methods. Parameters used in this example are the same as those in Section 3.1, $h = 2^{-5}$ and $\epsilon = 0.03\sqrt{2}$. Both of them provide the second order of accuracy; however, the SAFS starts to converge for a much bigger time step size and gives 2–3 more digits of accuracy where both methods in the convergence region.

4.2. Motion of a circle by its mean curvature

One of the well analyzed solutions of the AC equation is the motion of a circle. Suppose a radially symmetric initial condition is given as follows on the domain $\Omega = [0,1]\times[0,1]$,

$$\phi(x,y,0) = \tanh\frac{0.25 - \sqrt{(x-0.5)^2 + (y-0.5)^2}}{\sqrt{2}\epsilon}, \tag{19}$$

which represents a circle centered at $(0.5, 0.5)$ with a radius $R_0 = 0.25$. It is well known that the solution of the AC equation with the initial condition is radially symmetric and the radius of the interfacial circle (where $\phi(x,y,t) = 0$) is shrinking by the rate of the curvature of the circle.

We compute this two-dimensional problem with $\epsilon = 0.01$ using the second order SIFS (with $S = 2$) and SAFS methods on a regular 256×256 spatial grid. Fig. 6 shows the convergence rate of the solutions at $T_f = 0.0256$ by the methods. Here the error is computed by comparison with a quadruplely over-resolved numerical reference solution. Both of the methods converge with second order; however the SAFS starts to converge for a much bigger time step size and gives order of magnitude higher accuracy where both methods in the convergence region.

Asymptotic analysis shows that, in the limit that the radius of the circle is much larger than the interfacial thickness, the interfacial velocity $V(t)$ is given by

$$V(t) = \frac{dR(t)}{dt} = -\frac{d-1}{R(t)}$$

and the radius of the circle at time t can be computed as

$$R(t) = \sqrt{R_0^2 - 2(d-1)t} \quad \text{for } t \in [0, R_0^2/(2(d-1))], \tag{20}$$

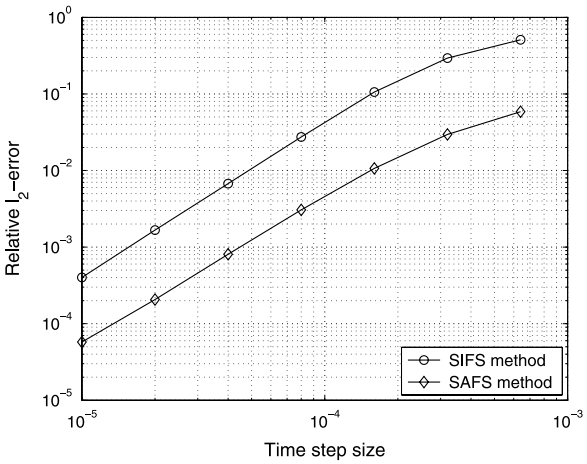

Fig. 6. Relative l_2 errors of the motion by curvature at $T_f = 0.0256$ by the SIFS and the SAFS methods for various time step sizes with $h = 2^{-8}$ and $\epsilon = 0.01$.

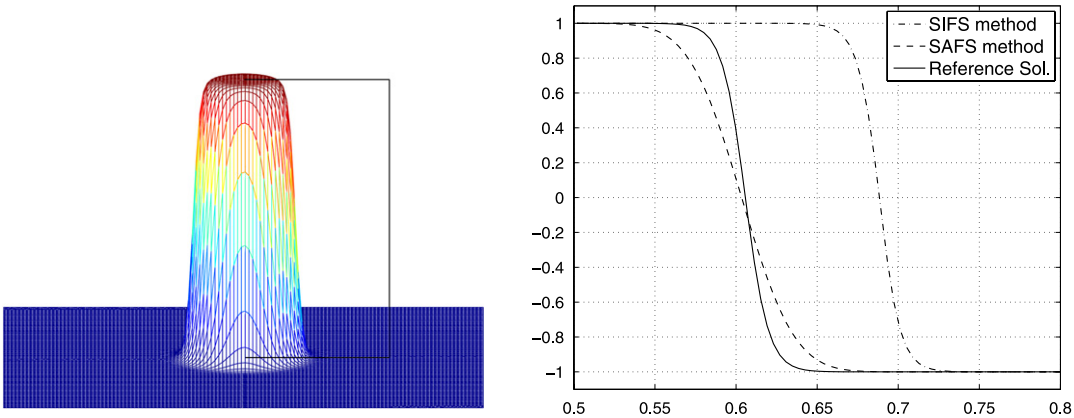

Fig. 7. Reference solution at $T_f = 0.0256$ and cross-section of the solution near the interface by the SIFS and the SAFS methods with $\Delta t = 6.4 \cdot 10^{-4}$.

where R_0 is the initial radius of the circle and d is the number of dimensions. The circle will shrink to the center of the circle and disappear for times larger than $R_0^2/(2(d-1))$.

Fig. 7 shows the reference solution at $T_f = 0.0256$ and two numerical solutions by the SIFS and the SAFS methods using a coarse time step $\Delta t = 6.4 \cdot 10^{-4}$. The interfacial circle of the SIFS solution slowly evolves in time and the computed radius $R = 0.1884$ at $T_f = 0.0256$ corresponds to the analytic solution at $t = 0.0135$. The radii of a circle as a function of time obtained from the SIFS and SAFS methods (using $\Delta t = 1.6 \cdot 10^{-4}, 3.2 \cdot 10^{-4}, 6.4 \cdot 10^{-4}$) are shown in Fig. 8(a) and (b), respectively. The SIFS method is quite accurate if a smaller time step is employed; however, at a larger time step, the SIFS method leads to a bad accuracy as compared to the analytical result. On the other hand, there is no visible difference between the numerical results obtained from the SAFS method and the analytical result even at larger time steps. This example numerically demonstrates that our SAFS method provides a second order of convergence and does not experience the time-delay side effect unlike the SIFS method.

4.3. Spinodal decomposition in 3-dimension

In this subsection, we perform a spinodal decomposition computation in 3-dimensional space using the second order SAFS method. The governing equation is again the AC equation derived in Section 3.2. We set $\epsilon = 0.015$ and $h = 1/64$ on the domain $\Omega = [0, 1] \times [0, 1] \times [0, 1]$ and the initial condition is $\phi(x, y, z, 0) = 0.005 \cdot \text{rand}(x, y, z)$ where $\text{rand}(x, y, z)$ is a random number between -1 and 1. We have checked that the method has the second order of convergence with respect to the time step size Δt and $\Delta t = 5 \cdot 10^{-4}$ for the computation is rather large but gives around a couple of digits of accuracy. Fig. 9 shows the computational results at $t = 0, 10^{-3}, 3 \cdot 10^{-3}, 6 \cdot 10^{-3}, 10^{-2}, 3 \cdot 10^{-2}$ with $\Delta t = 5 \cdot 10^{-4}$.

5. Conclusions

The stabilized semi-implicit Fourier spectral method is employed by many researchers since the stabilized semi-implicit scheme allows a much larger time step than a usual explicit scheme. But, we found that the first order stabilized semi-

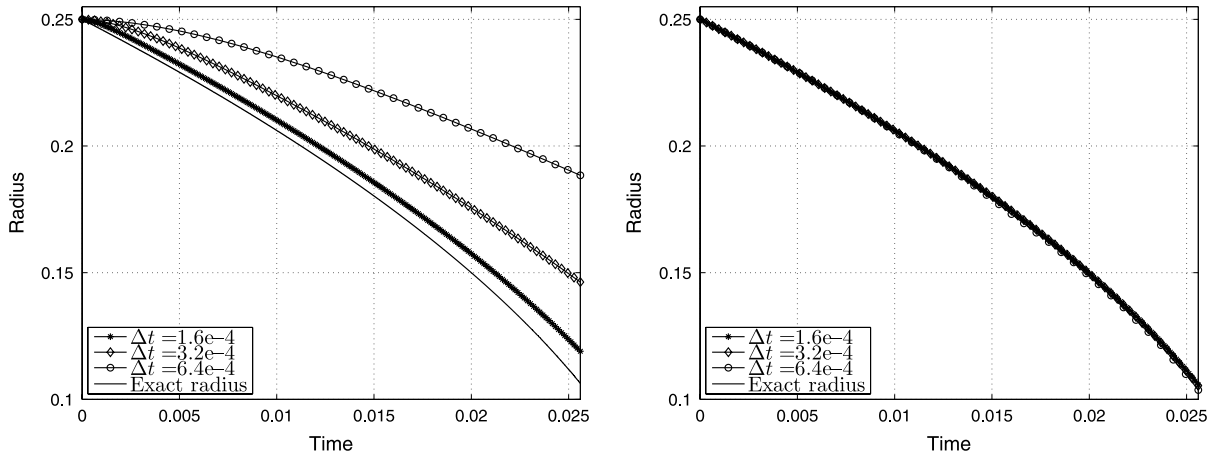

(a) Second order SIFS method. (b) Second order SAFS method.

Fig. 8. Radii of the interfacial circle as a function of time ($0 \le t \le 0.0256$) obtained by the SIFS and SAFS methods using $\Delta t = 1.6{\cdot}10^{-4}, 3.2{\cdot}10^{-4}, 6.4{\cdot}10^{-4}$.

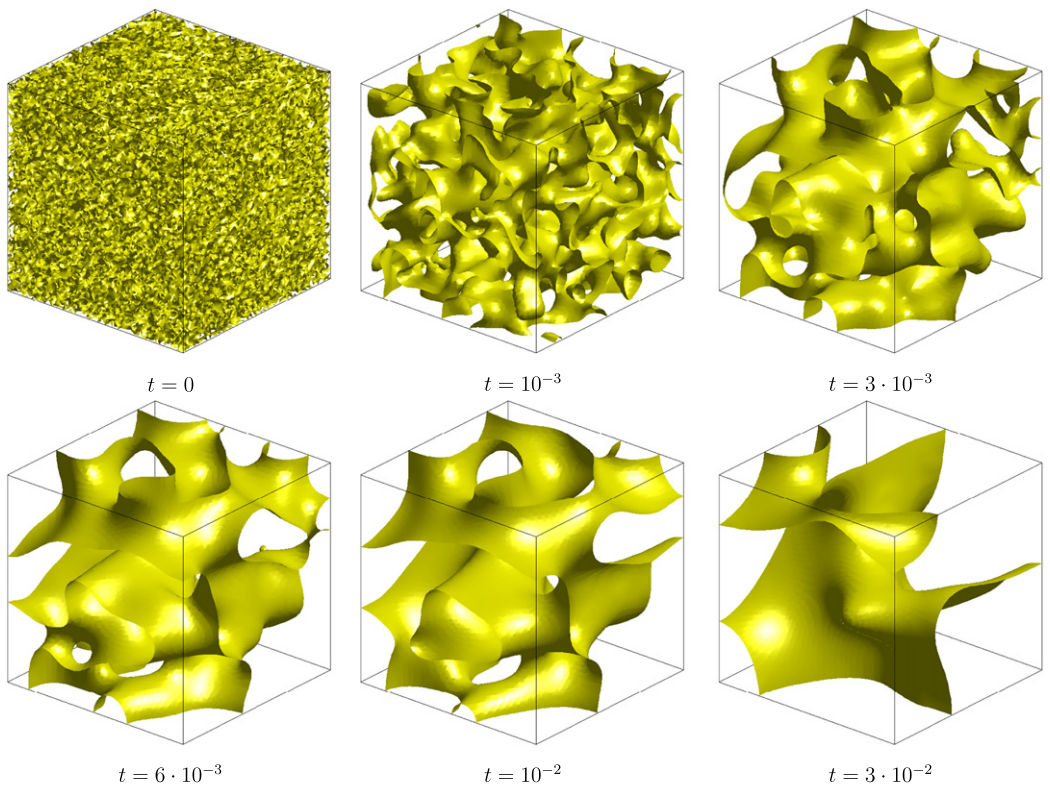

Fig. 9. Spinodal decomposition of the numerical solution $\phi(x, y, z, t)$ obtained from the second order SAFS method.

implicit scheme has a k_1k_2-dependent effective time step Δt_{eff} as $\Delta t_{\text{eff}} = \frac{\Delta t}{1-\Delta t A_{k_1k_2}+\frac{S\Delta t}{\epsilon^2}}$, where Δt is an algorithmic time step. This implies that the effective time step is identical to the algorithmic time step for small enough Δt. However, for a sufficiently large time step, the accuracy is significantly lost since $\Delta t_{\text{eff}} \ll \Delta t$ for $\Delta t \gg \frac{\epsilon^2}{S}$. In order to remove the time step constraint and guarantee the accuracy in time for a sufficiently large time step, we presented a semi-analytical Fourier spectral method for solving the Allen–Cahn equation. The core idea of this method was to decompose the original equation into linear and nonlinear subequations, which have closed-form solutions in the Fourier and physical spaces, respectively. This first order method is unconditionally stable and we demonstrated, through numerical experiments, that our proposed first order method is more accurate than the first order stabilized semi-implicit scheme. We also suggested a second order semi-analytical Fourier spectral method which is also unconditionally stable and more accurate than the well-known second

order stabilized semi-implicit method. We expect that our proposed methods can be used to solve various modified forms of the Allen–Cahn equation such as crystal growth, grain growth, and image analysis.

Acknowledgment

This research was supported by Basic Science Research Program through the National Research Foundation of Korea (NRF) funded by the Ministry of Education (2009-0093827, 2012-002298).

References

[1] V.E. Badalassi, H.D. Ceniceros, S. Banerjee, Computation of multiphase systems with phase field models, J. Comput. Phys. 190 (2003) 371–397.
[2] J.W. Cahn, J.E. Hilliard, Free energy of a nonuniform system. I. Interfacial free energy, J. Chem. Phys. 28 (1958) 258–267.
[3] D. Jacqmin, Calculation of two-phase Navier–Stokes flows using phase-field modeling, J. Comput. Phys. 155 (1999) 96–127.
[4] L.-Q. Chen, Phase-field models for microstructure evolution, Annu. Rev. Mater. Sci. 32 (2002) 113–140.
[5] H.G. Lee, J. Kim, A second-order accurate non-linear difference scheme for the N-component Cahn–Hilliard system, Physica A 387 (2008) 4787–4799.
[6] H. Gómez, V.M. Calo, Y. Bazilevs, T.J.R. Hughes, Isogeometric analysis of the Cahn–Hilliard phase-field model, Comput. Methods Appl. Mech. Engrg. 197 (2008) 4333–4352.
[7] S.-D. Yang, H.G. Lee, J. Kim, A phase-field approach for minimizing the area of triply periodic surfaces with volume constraint, Comput. Phys. Comm. 181 (2010) 1037–1046.
[8] H.G. Lee, J. Kim, Accurate contact angle boundary conditions for the Cahn–Hilliard equations, Comput. Fluids 44 (2011) 178–186.
[9] H.G. Lee, J.-W. Choi, J. Kim, A practically unconditionally gradient stable scheme for the N-component Cahn–Hilliard system, Physica A 391 (2012) 1009–1019.
[10] H.G. Lee, J. Kim, Numerical simulation of the three-dimensional Rayleigh–Taylor instability, Comput. Math. Appl. 66 (2013) 1466–1474.
[11] S.M. Allen, J.W. Cahn, A microscopic theory for antiphase boundary motion and its application to antiphase domain coarsening, Acta Metall. 27 (1979) 1085–1095.
[12] H. Garcke, B. Nestler, B. Stoth, A multiphase field concept: numerical simulations of moving phase boundaries and multiple junctions, SIAM J. Appl. Math. 60 (1999) 295–315.
[13] Z. Zhang, H. Tang, An adaptive phase field method for the mixture of two incompressible fluids, Comput. Fluids 36 (2007) 1307–1318.
[14] J.-W. Choi, H.G. Lee, D. Jeong, J. Kim, An unconditionally gradient stable numerical method for solving the Allen–Cahn equation, Physica A 388 (2009) 1791–1803.
[15] Y. Li, H.G. Lee, D. Jeong, J. Kim, An unconditionally stable hybrid numerical method for solving the Allen–Cahn equation, Comput. Math. Appl. 60 (2010) 1591–1606.
[16] N. Provatas, N. Goldenfeld, J. Dantzig, Efficient computation of dendritic microstructures using adaptive mesh refinement, Phys. Rev. Lett. 80 (1998) 3308–3311.
[17] P. Yue, C. Zhou, J.J. Feng, C.F. Ollivier-Gooch, H.H. Hu, Phase-field simulations of interfacial dynamics in viscoelastic fluids using finite elements with adaptive meshing, J. Comput. Phys. 219 (2006) 47–67.
[18] S. Wise, J. Kim, J. Lowengrub, Solving the regularized, strongly anisotropic Cahn–Hilliard equation by an adaptive nonlinear multigrid method, J. Comput. Phys. 226 (2007) 414–446.
[19] L.Q. Chen, J. Shen, Applications of semi-implicit Fourier-spectral method to phase field equations, Comput. Phys. Comm. 108 (1998) 147–158.
[20] C. Liu, J. Shen, A phase field model for the mixture of two incompressible fluids and its approximation by a Fourier-spectral method, Physica D 179 (2003) 211–228.
[21] P. Yue, J.J. Feng, C. Liu, J. Shen, A diffuse-interface method for simulating two-phase flows of complex fluids, J. Fluid Mech. 515 (2004) 293–317.
[22] W.M. Feng, P. Yu, S.Y. Hu, Z.K. Liu, Q. Du, L.Q. Chen, Spectral implementation of an adaptive moving mesh method for phase-field equations, J. Comput. Phys. 220 (2006) 498–510.
[23] R. Acar, Oscillation-free advection of interfaces with high order semi-Lagrangian schemes, Comput. Fluids 38 (2009) 137–159.
[24] R. Acar, Simulation of interface dynamics: a diffuse-interface model, Vis. Comput. 25 (2009) 101–115.
[25] A. Celani, A. Mazzino, P. Muratore-Ginanneschi, L. Vozella, Phase-field model for the Rayleigh–Taylor instability of immiscible fluids, J. Fluid Mech. 622 (2009) 115–134.
[26] J. Shen, X. Yang, An efficient moving mesh spectral method for the phase-field model of two-phase flows, J. Comput. Phys. 228 (2009) 2978–2992.
[27] G. Tegze, G. Bansel, G.I. Tóth, T. Pusztai, Z. Fan, L. Gránásy, Advanced operator splitting-based semi-implicit spectral method to solve the binary phase-field crystal equations with variable coefficients, J. Comput. Phys. 228 (2009) 1612–1623.
[28] X. Yang, Error analysis of stabilized semi-implicit method of Allen–Cahn equation, Discrete Contin. Dyn. Syst. Ser. B 11 (2009) 1057–1070.
[29] J. Shen, X. Yang, Numerical approximations of Allen–Cahn and Cahn–Hilliard equations, Discrete Contin. Dyn. Syst. Ser. A 28 (2010) 1669–1691.
[30] X. Yang, M.G. Forest, C. Liu, J. Shen, Shear cell rupture of nematic liquid crystal droplets in viscous fluids, J. Non-Newton. Fluid Mech. 166 (2011) 487–499.
[31] M. Cheng, A.D. Rutenberg, Maximally fast coarsening algorithms, Phys. Rev. E 72 (2005) 055701(R).
[32] R. Kobayashi, Modeling and numerical simulations of dendritic crystal growth, Physica D 63 (1993) 410–423.
[33] A. Karma, W.-J. Rappel, Quantitative phase-field modeling of dendritic growth in two and three-dimensions, Phys. Rev. E 57 (1998) 4323–4349.
[34] L.-Q. Chen, W. Yang, Computer simulation of the domain dynamics of a quenched system with a large number of nonconserved order parameters: the grain-growth kinetics, Phys. Rev. B 50 (1994) 15752–15756.
[35] I. Steinbach, F. Pezzolla, B. Nestler, M. Seeßelberg, R. Prieler, G.J. Schmitz, J.L.L. Rezende, A phase field concept for multiphase systems, Physica D 94 (1996) 135–147.
[36] R. Kobayashi, J.A. Warren, W.C. Carter, A continuum model of grain boundaries, Physica D 140 (2000) 141–150.
[37] D. Mumford, J. Shah, Optimal approximations by piecewise smooth functions and associated variational problems, Comm. Pure Appl. Math. 42 (1989) 577–685.
[38] T.F. Chan, L.A. Vese, Active contours without edges, IEEE Trans. Image Process. 10 (2001) 266–277.
[39] M. Beneš, V. Chalupecký, K. Mikula, Geometrical image segmentation by the Allen–Cahn equation, Appl. Numer. Math. 51 (2004) 187–205.
[40] T.F. Chan, S. Esedoğlu, M. Nikolova, Algorithms for finding global minimizers of image segmentation and denoising models, SIAM J. Appl. Math. 66 (2006) 1632–1648.
[41] S. Esedoğlu, Y.-H.R. Tsai, Threshold dynamics for the piecewise constant Mumford–Shah functional, J. Comput. Phys. 211 (2006) 367–384.
[42] J.A. Dobrosotskaya, A.L. Bertozzi, A wavelet-Laplace variational technique for image deconvolution and inpainting, IEEE Trans. Image Process. 17 (2008) 657–663.
[43] D.A. Kay, A. Tomasi, Color image segmentation by the vector-valued Allen–Cahn phase-field model: a multigrid solution, IEEE Trans. Image Process. 18 (2009) 2330–2339.
[44] Y. Li, J. Kim, Multiphase image segmentation using a phase-field model, Comput. Math. Appl. 62 (2011) 737–745.
[45] N. Ahmed, T. Natarajan, K.R. Rao, Discrete cosine transform, IEEE Trans. Comput. C-23 (1974) 90–93.
[46] E.V.L. de Mello, O.T. da Silveira Filho, Numerical study of the Cahn–Hilliard equation in one, two and three dimensions, Physica A 347 (2005) 429–443.
[47] P.C. Fife, Models for phase separation and their mathematics, Electron. J. Differential Equations 2000 (2000) 1–26.